Chemical Physics xxx (2013) xxx–xxx

Contents lists available at SciVerse ScienceDirect

Chemical Physics

journal homepage: www.elsevier.com/locate/chemphys

$NO + NH_3$ reaction over polycrystalline Pt: Numerical analysis of spatio-temporal data and evidence of non-linear behavior

M. Rafti *, A.G. Albesa, J.L. Vicente

Instituto de Investigaciones Fisicoquímicas Teóricas y Aplicadas (INIFTA-CONICET), Dpto. Química, Universidad Nacional de La Plata, La Plata, Argentina

ARTICLE INFO

Article history:
Received 17 September 2012
In final form 14 December 2012
Available online xxxx

Keywords:
Catalytic Surface Reactions
Ammonia oxidation
Platinum poly and single crystals
Photoelectron Emission Microscopy (PEEM)
Nonlinear phenomena

ABSTRACT

Surface catalytic reactions display under low pressure conditions non-linear features such as non-stationary reaction rates and spatio-temporal patterns known as dissipative structures. We analyze experimental data from ammonia oxidation reaction over polycrystalline platinum catalyst using quantitative and qualitative nonlinearity tests, such as the Grassberger–Procaccia (GP) algorithm and Surrogate Time Series. Analyses were conducted using local and global information; additionally, we present evidence confirming previously proposed mechanism for the reaction system.

1. Introduction

The catalytic ammonia (NH_3) oxidation with several agents such as nitrous oxide (NO) and molecular oxygen (O_2) over different crystallographic faces of platinum (Pt) and other d-band transition metals was intensively explored recently. A detailed description of the complex behavior observed can be founded in several experimental studies and numerical simulations carried for near-UHV (ultra high vacuum) conditions; see e.g. Refs. [1–7] respectively. Single crystals used as model catalysts offer a great deal of control on structure, from which valuable information can be inferred. Nevertheless, a crucial shortcoming of the approach is a lack of agreement when extrapolating results obtained for these rather ideal systems to conditions typically used for industrial applications. One of the main reasons is that when catalysts are subjected to severe temperature and pressure conditions, polycrystalline structures are likely to emerge after short reaction periods due to high atom mobility, the problem is known as the *material gap*. Catalytic reactions carried over single crystal d-band transition metal surfaces were found to display non-linear features such as non-stationary time evolution in product formation rates, and coverages of intermediate adspecies. Furthermore, spatio-temporal patterns (i.e., *dissipative structures* [8]) were detected when using surface sensitive imaging techniques such as Photoelectron Emission Microscopy (PEEM) [9,10]. Briefly, PEEM reflects local changes in surface work-function (wf), which in turn can be related to the presence of adsorbates known to cause these modifications (wf enhancement provokes darkening of the image obtained due to a lower photoelectron yield, and vice versa).

The problem of qualitatively establish the nature of the observed dynamics is far from trivial, and a number of tools for nonlinear time series analysis are suitable for this purpose; e.g., determination of embedding dimension of the phase space attractor, or surrogate test [11,12].

In an attempt to overcome the above discussed material gap, polycrystalline Pt catalysts were used in several experimental studies; see e.g. Takoudis and Schmidt [13,14], Katona and Somorjai [15], and McMillan et al. [16]. We analyzed data presented in Ref. [16] which corresponds to PEEM and reaction rate measurements carried via quadrupole mass spectrometry (QMS) for the $NO + NH_3$ reaction in the 1×10^{-4} mbar and 460—520 K pressure–temperature ranges over polycrystalline Pt catalyst. McMillan et al. reported the appearance of spontaneous reaction rate oscillations and dissipative structures, which the authors speculated to be caused by coupling between large number of multi-modal oscillators constituted by grains with different crystallographic orientations. Given previous experimental evidence, this is a valid hypothesis; nevertheless, it also gives rise to many additional questions which we seek to answer in the present manuscript by applying proper numerical analysis. Namely; are all these oscillators substantially similar or can be grouped according to some criterion? What is the relation between global and local behavior? And related to this point, what is the coupling mechanism operating between grains on the polycrystal; it is local (via surface diffusion), or global (via gas phase synchronization)?

* Corresponding author.
E-mail address: mrafti@quimica.unlp.edu.ar (M. Rafti).

0301-0104/$ - see front matter © 2012 Elsevier B.V. All rights reserved.
http://dx.doi.org/10.1016/j.chemphys.2012.12.019

The $NO + NH_3$ reaction follows a predominant pathway on the (100) face of Pt. Reduction of NO to N_2 was observed in previous work carried by Vesser et al. [1]:

$$6NO + 4NH_3 \rightarrow 5N_2 + 6H_2O$$

It was proposed recently [4], that the accepted Lombardo–Fink–Imbihl (LFI) [2] mechanism for the reaction system (a system of seven coupled ordinary differential equations (ODE) describing temporal evolution of coverages and reaction rates) can be reduced via adiabatic elimination of fast variables. We use the present analysis of time series to assess the validity of both the LFI mechanism and the possibility of such adiabatic reduction.

The remainder of this work is organized as follows. Main experimental features of the system studied and data used for analysis are described in Section 2, methods employed for time series acquisition from video files are discussed in Section 3. Section 4 is devoted to present tests used for non-linearity detection; and finally, discussion of results and conclusions are given in Section 5.

2. $NO + NH_3 - Pt$: main experimental findings

Experiments carried by McMillan et al. [16] in which, for constant gas phase composition, temperature of the polycrystalline Pt catalyst was ramped up and down, revealed hysteresis on reaction rates; which is qualitatively similar to previous reports on similar systems [2]. Specifically, via spatially resolved (PEEM) and integral (QMS) measurements the authors reported pattern formation (reaction fronts and clustering) and irregular reaction rate oscillations for a wide temperature window (460—520 K) and gas phase reactant mixture composition $(p_{NO} : p_{NH_3}) = (0.2 - 0.8)$ (total pressure $\approx 1 \times 10^{-4}$ mbar).

Following Katona and Somorjai [15], one can consider the Pt polycrystal surface as constituted mainly of (100) and (111) faces. There are a number of well-known processes occurring when adspecies such as NO, O, or CO are present on these surfaces.

- The Pt (100) grains participate actively in the $NO + NH_3$ reaction, while the Pt (111) grains are mainly inactive. This is due mainly to both the low sticking coefficient of ammonia, and the low dissociation probability of NO on Pt (111) [17,18].
- Pt (100) face is known to suffer a surface reconstruction upon critical coverage of NO and O adspecies, which switches between two states of high and low catalytic activity [19,2], the so-called (1×1) and hex (reconstructed) phasess respectively.
- For temperature cycling experiments, a difference in catalytic activity between heating (high) and cooling (low) stages is observed. This can be attributed to the fact that NO adsorption dominates initial low temperature state, and under these conditions the surface is mainly in the (1×1) state. Upon heating, the surface is depleted of NO by reaction (an autocatalytic process known as *surface explosion* [2]), and once coverage falls below a critical limit, hex reconstruction takes place together with a drop in activity.

In particular, for Pt (100), a rich variety of complex behavior ranging from homogeneous oscillations to pseudo-chaotic variations on reaction rates and surface coverages, together with spatio-temporal patterns were reported. Imbhil et al. [1] proposed a detailed mechanism which describes observed dynamics, the so called LFI mechanism with seven intermediate adspecies. Simulations carried using the LFI mechanism for both mean field [4] and spatially extended approximations [6,7,5] demonstrated that despite the approximations made, the model can capture fundamental features of the experimental system. Furthermore, the possibility of an adiabatic reduction was demonstrated in Ref. [4].

3. Image and data processing

3.1. PEEM

Spatially resolved experimental information was obtained from PEEM RGB-videos recorded using a CCD camera under reaction conditions, total image wide 500 μm. The imaged area was considered to be representative of the complete polycrystalline sample, this assumption was confirmed comparing local (PEEM) and global (QMS) behavior (for further details see Ref. [16]). Considering maximum spatial resolution (1 pixel ≈ 1.5 μm) and the already known propagation speed of reaction fronts ($\approx 1\,\mu m\,s^{-1}$ [1]); a reduction from the original recording frame rate of 30–4 fps was performed. This reduces considerably the volume of data to be handled and improves the speed of calculations made, without any detriment to the significance of results obtained. RGB intensities were converted to 0–255 gray-scale, from which time series of any selected sampled area can be constructed using software specially developed for such purpose.

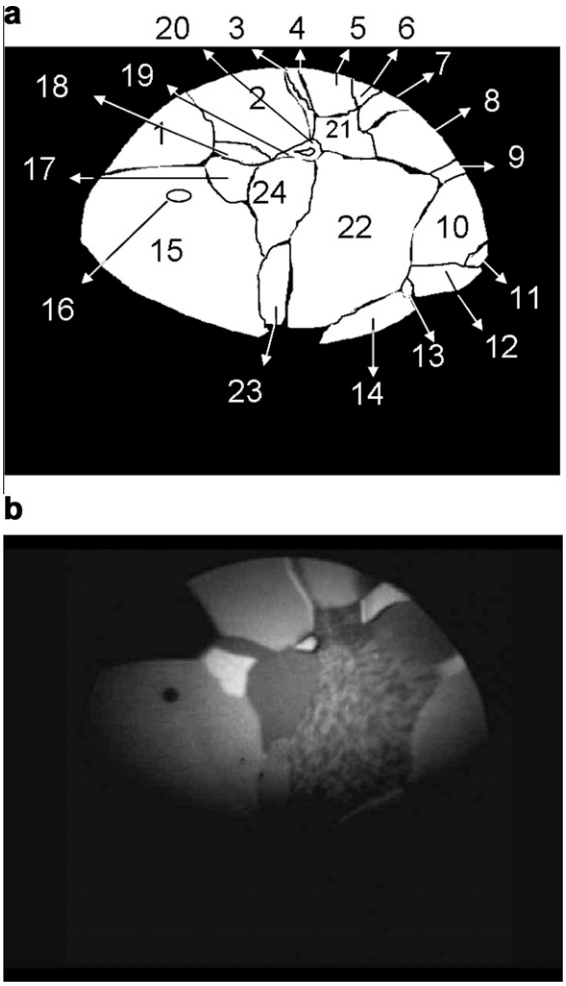

Fig. 1. (a) Clock-wise labeling applied to different areas in the image corresponding to PEEM snapshot presented in (b). (b) Typical snapshot from PEEM video files processed under reaction conditions. Gray scale represents surface work-function values, bright can be associated to ammonia covered areas, while dark grains to mainly NO/O covered surface. Image wide 500 μm.

Table 1
Classification of grains according to time series analysis, and proportional area of the total sampled area represented.

Class	Label	Surface percentage
Type I	6, 8, 12, 21, 22, 24	47.23
Type II	1, 4, 10, 11, 13, 14, 15, 16, 18, 19, 23	15.76
Type III	2, 3, 5, 7, 9, 17, 20	37.01

Several grains show oscillations, while other appear to be inactive and remain in a fixed bright or dark state (with slight changes in brightness attributable to background). A typical snapshot taken from PEEM video files, and the labeling applied to different areas can be observed in Fig. 1.

It was assumed, following McMillan et al. [16], that areas showing catalytic activity belonged mainly to (100) orientation. When analyzing time series extracted from each labeled area, three groups with different characteristic behavior emerged, namely Areas type I–III:

- Areas type I, feature multi-peaked temporal oscillations with intensity amplitude changes greater than 0.2 brightness units (normalization fixed scale used was $0\,(dark) \rightarrow 0$, and $1\,(bright) \rightarrow 255$).
- Areas type II, remain in a dark state (intensity < 0.3).
- Areas type III, always in a bright state (intensity > 0.65).

Table 1 summarizes grain classification based on time series behavior above discussed, together with percentage of total area that each type represents. Fig. 2 display examples of time series from type I–III areas.

3.2. QMS: rate measurements

Time series can be also constructed using global information from QMS experiments. In this way, relative influence of coupling between different areas of the catalytic surface can be assessed. Both reaction products (N_2 and H_2O) could be used in principle for the analysis since the reaction rates are synchronized; N_2 was selected due to the higher relative intensity. Smoothing and $0-1$ re-normalization was carried as can be observed in Fig. 3.

3.3. Time Series analysis

Type I areas (which interestingly are not necessarily nearest-neighbors, see Fig. 1) display multi-peaked oscillations. A natural question to ask would be if all the areas belonging to this class feature the same dynamics; or, if this observed behavior arise instead from some kind of superposition of oscillating subgroups within type I. Comparison between local (PEEM) and global (QMS) data allows for a further classification into two subgroups; areas labeled 12 and 22, (from now on type I-A) displaying multi-peak oscillations with large period (≈ 60 s); and areas 6, 8, 21 and 24 (labeled as type I-B), with approximately half-length oscillation period (≈ 30 s). This is depicted in Fig. 4 where time series and power spectrum are displayed.

Power transfer from 30 s and 15 s peaks in type I-B areas to new 20 s and 60 s. period peaks corresponding to type I-A power spectrum, evidence a different behavior for each subgroup. Regarding surface coverage changes during a cycle, Fig. 5 displays a more detailed description of transformations for neighboring type I-A and I-B areas, where snapshots of time evolution are presented. Interestingly, short-period oscillation areas (type I-A) can be related to spatially homogeneous PEEM intensity changes (upper snapshot sequence in Fig. 5); while the long-period oscillations (type I-B, lower snapshot sequence in Fig. 5) occur together with cluster-like pattern formation (resembling what was obtained in simulations for the $NO + NH_3 - Pt(100)$ using the LFI model, see Ref. [6,7]).

3.4. Time Series and LFI mechanism

Previous numerical simulations of the reaction system [4] were carried using proposed intermediate species and kinetic constants taken from the LFI mechanism [1,2]. As discussed above, LFI mechanism was developed to describe experimental observations based upon the decisive role of the adsorbate induced $1 \times 1 \rightleftharpoons$ hex phase transition known to occur for Pt (100) single crystal surface. A set of seven coupled ordinary differential equations (ODE) allows describing time evolution of adsorbates and percentage of the catalytic surface in either 1×1 or hex phases. Using an ODE system implies to assume homogeneous distribution of adsorbates (the equivalent of continuously stirred tank reactors or CSTR in liquid phase reactions); therefore it is not appropriate to model spatio-temporal behavior (i.e., experimental data arising from spatially resolved and surface sensitive techniques such as PEEM), because of the non-homogeneous distributions that need to be considered. A widely used approach to such problem, after pioneering work of Ertl [20], is to model the surface as composed of subsystems (or *cells*) small enough to ensure that application of mean field hypothesis is valid within these domains (i.e., no spatial gradient of adsorbate distributions). The next step is to apply diffusional coupling between adjacent cells, thus obtaining the so called *reaction-diffusion* equations; a set of Partial Differential Equations (PDE). Ordinary Fickean diffusion was shown to be successful in many systems

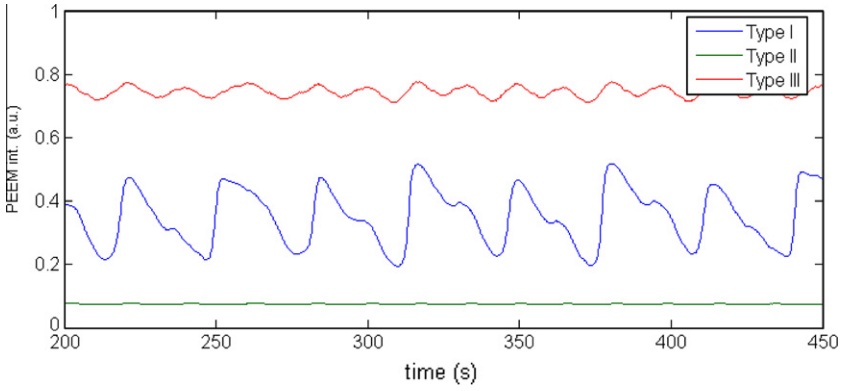

Fig. 2. Time series extracted from areas type I, II and III corresponding to PEEM image in Fig. 1. Distinctive behavior can be observed, with type II alone featuring true multi-peaked oscillations on brightness level. Experimental conditions: $p_{tot} = 1.6 \times 10^{-4}$ torr,*mhboxNO*/$NH_3 = 0.5$, and $T = 477$ K.

Please cite this article in press as: M. Rafti et al., Chem. Phys. (2013), http://dx.doi.org/10.1016/j.chemphys.2012.12.019

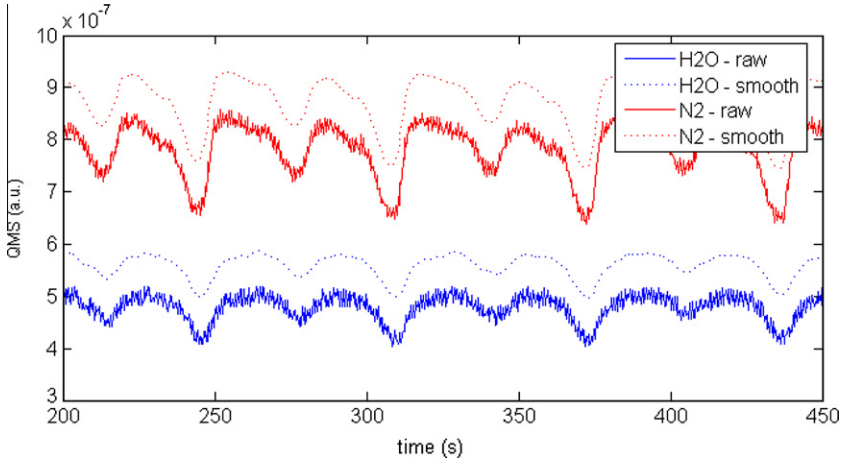

Fig. 3. Example of raw and smoothed QMS time series for reaction products N_2, $m/e = 28$ and H_2O, $m/e = 18$ displaying multi-peaked oscillations. Same experimental conditions as in Fig. 2.

[21], but non-Fickean diffusion was needed in order to accurately describe phenomena like site-blocking due to interactions among adsorbates [5,22,23].

The choice of an optimal length for spatial discretization is a non-trivial task; the use of a value smaller than the lower limit set by experimental technique resolution (for PEEM, a few μm) would bring only slower calculation performances and numerical problems related to the integration of the differential equations. On the other hand, if spatial discretization is made using an excessively large parameter, important features of the real system could be smeared out. In previous simulations works, experimental features observed via PEEM were reproduced using a cell dimension of 2.5 μm^2 [5–7]. Using data extracted from type I-A areas (cluster-like patterns) the above discussed hypothesis was tested. Two increasingly smaller circularly shaped sub-areas labeled as *sub*1 and *sub*2 were selected randomly from area 22 (Fig. 5 lower

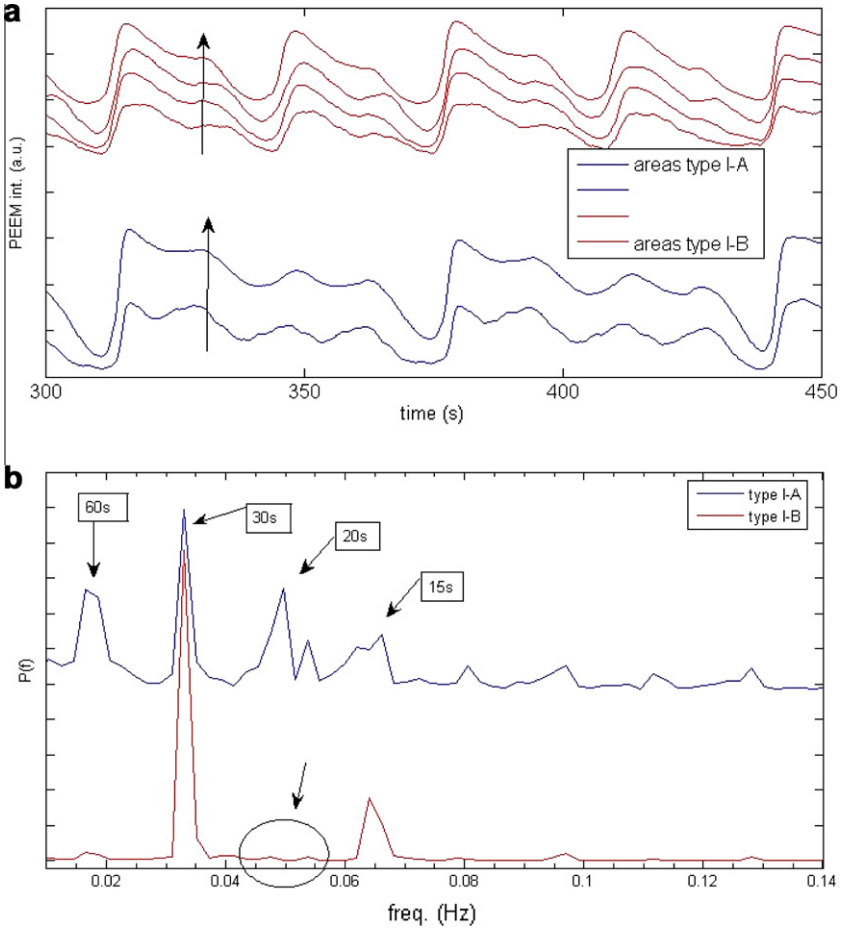

Fig. 4. (a) Local time series from PEEM experiments, type I-A (12 and 22, blue) and type I-B (6, 8, 21, and 24, red) subgroups. Arrows indicate the direction of increasing label area number in each subgroup. (b) Power spectrum constructed from time series, which evidences the different behavior observed; i.e., presence of the 60 s. peak only in type I-A, and absence of the 20 s. peak in type I-B. (For interpretation of the references to color in this figure legend, the reader is referred to the web version of this article.)

Please cite this article in press as: M. Rafti et al., Chem. Phys. (2013), http://dx.doi.org/10.1016/j.chemphys.2012.12.019

panel). Diameter of *sub*1 and *sub*2 areas ($d = 21$ μm, and $d = 4.5$ μm respectively) were selected bearing in mind typical size of surface structures observed in PEEM experiments ($d \approx 20$—25 μm). Results can be observed in Fig. 6, and the fact that shape of time series is preserved even when spot sizes of less than half cluster diameter were used, confirms the suitability of the scaling proposed in previous simulations attempts.

Time series obtained from type I-A and I-B (PEEM) were compared with global rate measurements (QMS); Fig. 7 illustrates the results obtained. According to the LFI mechanism, PEEM high brightness areas (low surface work function) correspond to NH_X ($x = 0 - 2$)-covered, catalytically active 1×1 phase; while dark areas (high work function) remain in an inactive state, mainly oxygen covered hex phase [1]. The comparison yields a nice confirmation of the above discussed correlation between catalytic activity and PEEM brightness, even though analyzed data was obtained from polycrystalline Pt surface. Additionally, Fig. 7 allows for further discussion on the relation between local and global behavior; this is, how the different classes of oscillatory regimes described in Section 3.3 interact to give raise to the global behavior. Remarkably, QMS signal cannot be reproduced neither by using PEEM type I-A nor type I-B time series alone; instead, signal best fit was obtained using a linear combination of both area types using as coefficients the occupation percentages as taken from PEEM (see Fig. 1, ≈ 0.65 for type I-A and ≈ 0.35 for type I-B):

$$Total\ signal = a * signal(\text{type I} - \text{A}) + b * signal(\text{type I} - \text{B})$$

$$a = \frac{Area(\text{type I} - \text{A})}{Area(\text{type I})}; \quad b = \frac{Area(\text{type I} - \text{B})}{Area(\text{type I})}.$$

Based on the above discussion, it can be concluded that different processes operate in each subgroup, and that collective behavior arises merely as a superposition without any synergy or feedback taken place, contrary to what was previously hypothesized.

4. Qualitative and quantitative non-linear tests

4.1. Grassberger–Procaccia algorithm for fractal dimension analysis

In order to detect the underlying dynamics of a complex system such as the one under study, the question of whether a subgroup of *fundamental* variables of the *a priori* needed set, can be used to correctly describe time evolution is crucial. As was discussed in Section 2, models proposed for description of NO and NH_3 surface catalytic reaction, involve seven coupled differential equations (LFI model). Numerical attempts aimed to detect this subset of variables were performed via the adiabatic elimination procedure [4]. The application of such procedure, allowed the authors to propose that system time evolution could be successfully represented using only a subset of three fundamental variables. A suitable way to test the validity of the above discussed prediction would be to determine the embedding dimension of the so-called *phase-space* attractor from time series. The applicability of the adiabatic elimination procedure and the identification of the fundamental variables to describe a complex system may be also deduced in principle from the exact macroscopic equations (if available) without need to analyze experimental data or carry out experiments.

Generically, the phase space is an abstract mathematical space spanned by the system observables. The state of the system at a given instant in time can be represented by a point in this phase space. If there are n variables then the space would be an Euclidean R_n space, and time evolution of the system will be a trajectory in this phase space. The object described by the trajectory can be measured in terms of the space-filling dimension d; e.g., if d is an integer number then the object is a point ($d = 0$), a line ($d = 1$), a plane ($d = 2$), etc. If the system displays chaotic behavior, then trajectories in the phase space will wander forever onto a so-called *strange attractor*, never repeating previous positions. Because of the above discussed definition, strange attractors are fractal

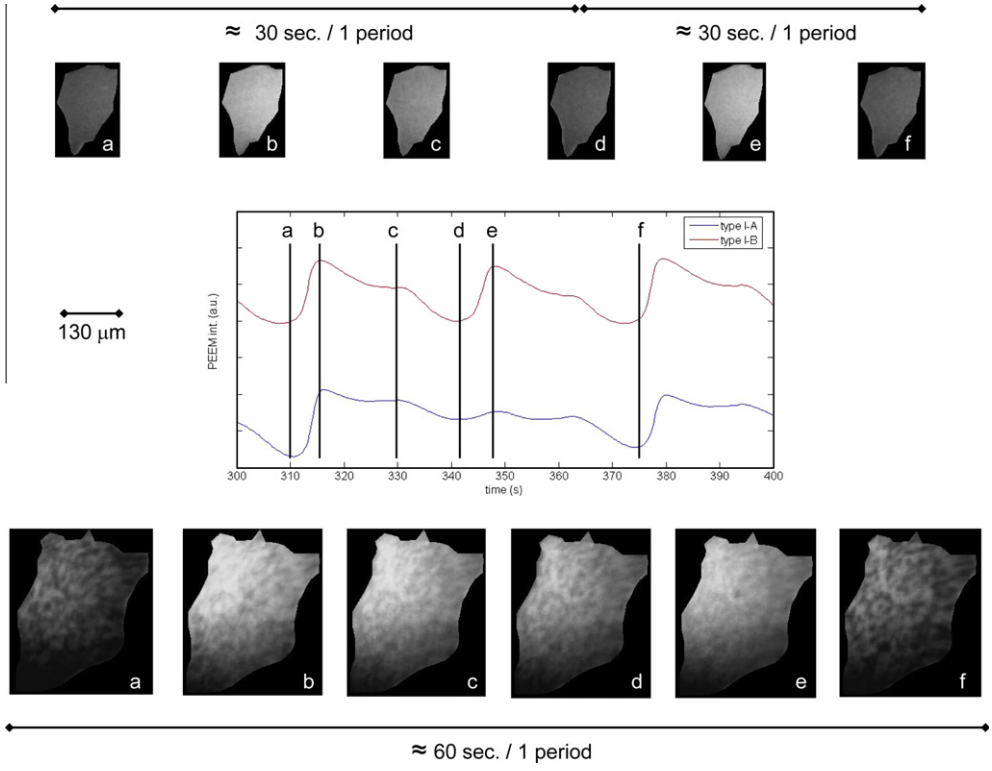

Fig. 5. Center panel shows PEEM time series for type I-A (blue) and type I-B (red) subgroups. Vertical lines labeled (a) through (f) indicate stages in time evolution in which snapshots for red (top panel, area 24 in 1) and blue (bottom panel, area 22) time series were taken from experiments. Spatial scale as displayed center left panel. (For interpretation of the references to color in this figure legend, the reader is referred to the web version of this article.)

Please cite this article in press as: M. Rafti et al., Chem. Phys. (2013), http://dx.doi.org/10.1016/j.chemphys.2012.12.019

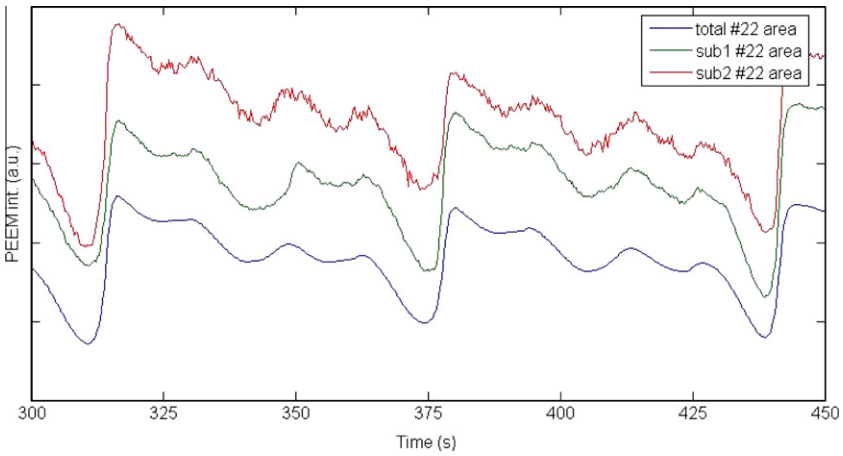

Fig. 6. Time series constructed with two circularly-shaped subareas randomly taken from area 22 (type I-A) in PEEM experiments (see Fig. 1). Label *sub*1 corresponds to diameter $d = 21$ μm and *sub*2 to $d = 4.5$ μm. For reference, time series constructed with the whole averaged area 22 as it appears in Fig. 5, is also displayed.

objects; i.e., non-integer values arise when calculating correlation dimension; and the minimum number of variables needed to describe the temporal evolution of the system is simply related to it. We used the Grassberger–Procaccia (GP) algorithm to determine the correlation dimension of the attractor [11,24] obtained from PEEM and QMS time series. Results of this procedure are shown in Fig. 8.

If white Gaussian noise is considered, an unbounded increase in correlation dimension when increasingly higher embedding dimensions are used is expected (i.e., the trajectory in the phase

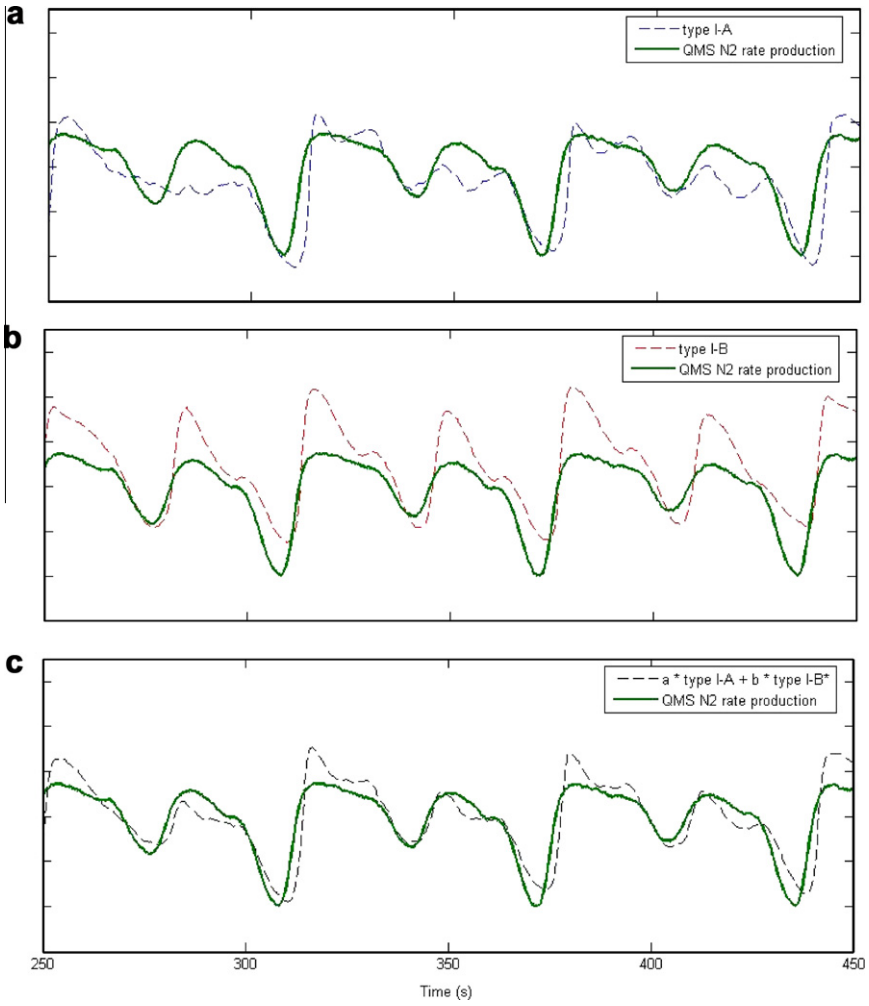

Fig. 7. Comparison between QMS N_2 rate measurements (full line) and PEEM intensity as extracted from (a) type I-A, (b) type I-B and (c) a linear combination using percentage of areas as *a* and *b* coefficients (broken line). Experimental conditions corresponding to time series presented in Fig. 2.

Please cite this article in press as: M. Rafti et al., Chem. Phys. (2013), http://dx.doi.org/10.1016/j.chemphys.2012.12.019

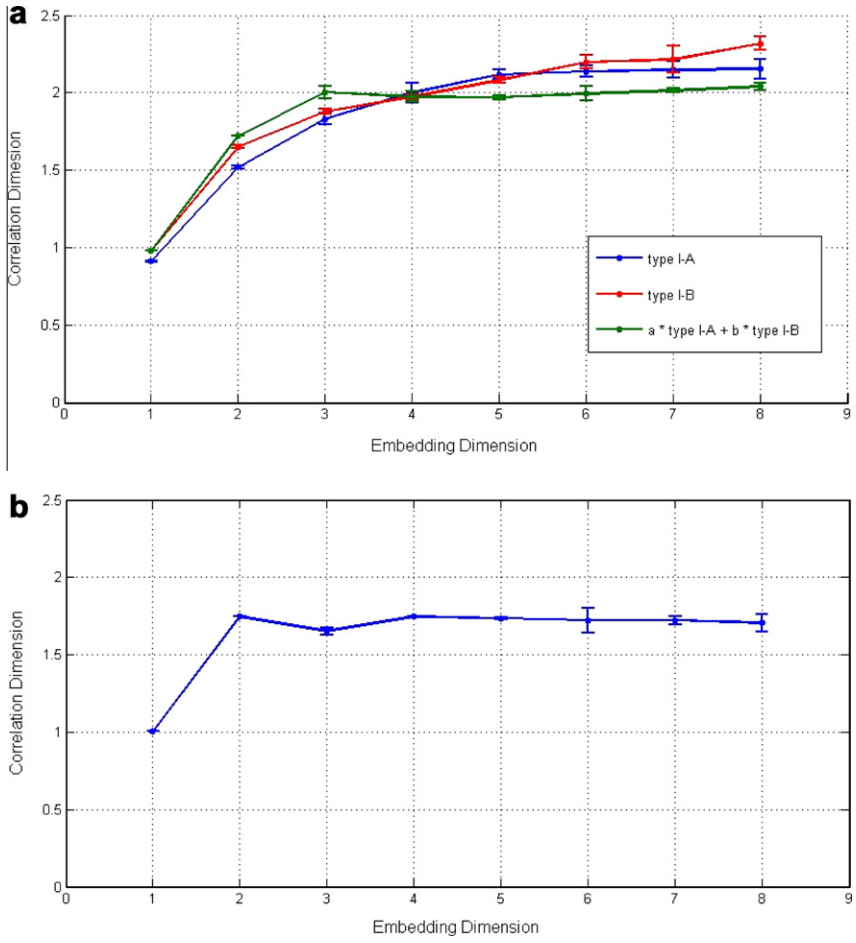

Fig. 8. (a) Correlation dimension versus embedding dimension plots for PEEM type I-A, type I-B and the linear combination of both areas (using same *a* and *b* coefficients as in Fig. 7). (b) The same plot for global N_2 QMS signal.

space would span over the whole available space for a given dimension). Remarkably, it can be inferred from Fig. 8(a) that the system reaches a plateau for embedding dimension (*x*-axis) ≈ 4—5; the criteria widely used is that correlation dimension should stay within 10% of the limit value when using two consecutive embedding dimension values. The non-integer correlation dimension value founded alone is not sufficient evidence to ensure chaotic behavior, because the GP algorithm is meant to be used as a confirming tool more than a detecting algorithm [25]. For example, Osborne and Provenzale [26], and Rapp et al. [27] showed that time series constructed using a simple class of colored random noise yields a GP finite fractal correlation dimension value which mimics what is expected for low-dimensional chaotic attractors. Nevertheless, the above mentioned finding constitutes an indicator of the minimum number of variables needed to form a space in which the trajectory followed by the system evolution can be contained. For type I-A and type I-B, this number was found to be three, which supports the existence of a subset of three fundamental variables

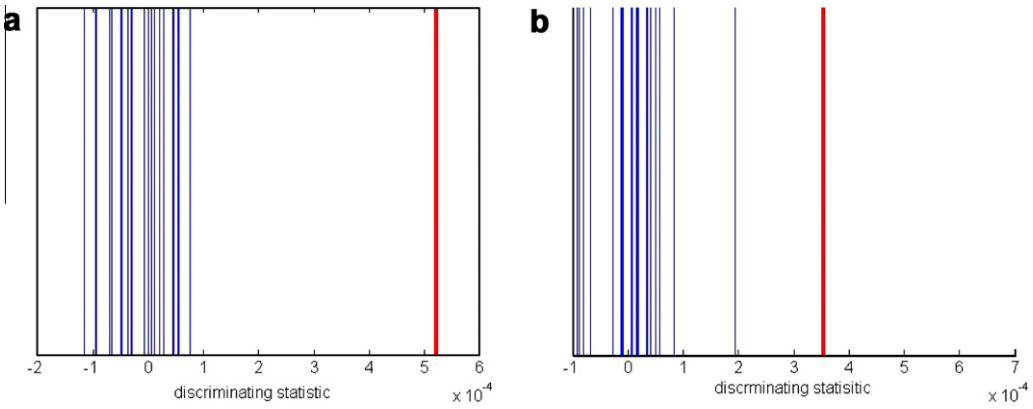

Fig. 9. Surrogate test for non-linearity in (a) PEEM type I-A, and (b) type I-B. Red bold line is the discriminating statistic value for the experimental data, while the blue lines represent the 39 surrogate data sets in each case. (For interpretation of the references to colour in this figure legend, the reader is referred to the web version of this article.)

Please cite this article in press as: M. Rafti et al., Chem. Phys. (2013), http://dx.doi.org/10.1016/j.chemphys.2012.12.019

in the LFI mechanism needed to describe system time evolution [4]. The GP plots obtained for the linear combination of PEEM and QMS signals displayed in Fig. 8(b) would indicate a number of variables needed of two, which can be rationalized as a complexity loss due to coupling and smearing out when going from local to globally measured time series.

4.2. Surrogate test for non-linear behavior detection

To quantitatively address the issue of whether the system can be classified as non-linear, surrogate test was applied [28,12]. The procedure can be summarized as follows; a suitable null hypothesis is formulated for the underlying process; (e.g., *the process is linear*) then it is accepted or rejected given that the test data is likely to have resulted from that premise or not. This is done by computing a discriminating statistic (also called test criterion) from the test data and then inquiring whether the computed value is compatible with the null hypothesis posed. The discriminating statistic is determined from an ensemble of randomized time series that accurately represent the null hypothesis (the surrogate data ensemble), and then its distribution is compared with the calculated value from test data. If it lies within the distribution, null hypothesis is accepted, otherwise is rejected.

For the test, 39 amplitude-adjusted Fourier transform (AAFT) surrogate time series were generated, and a discriminating statistic which computes the asymmetry due to time reversal was selected [29,28]. If probabilistic properties of a time series are invariant after time reversal transformation, then it can be classified as reversible; otherwise it is irreversible. This in turn also means that such time series can be regarded as a realization of a linear random process with independent identically distributed Gaussian noise. Rejection of the null hypothesis based on the above discussed discriminating statistic implies the contrary; i.e., that the process is not linear.

By construction, the probability of erroneously rejecting the null hypothesis is 5% (the so called size of the test). In Fig. 9 results of the above described analysis are showed, the discriminating statistic was calculated using the 39 surrogate ensemble (blue lines), and then compared to the result obtained using the data arising from PEEM time series (red line). Rejection of the null hypothesis was observed in both cases and consequently, type I-A and type I-B data sets can be classified as non-linear according to surrogate test criterion.

5. Conclusions and outlook

Local and global experimental data for temporal behavior during the catalytic surface reaction of ammonia with NO over a platinum polycrystal catalyst was analyzed in the range of temperatures (460–520 K) and gas phase reactant mixture composition ($p_{NO} : p_{NH_3}$) = (0.2 – 0.8) (total pressure $\approx 1 \times 10^{-4}$ mbar).

The validity of assumptions made in previous simulation attempts for related systems, and the suitability of the LFI model to describe dynamics were confirmed. Analyzing increasingly smaller areas taken from PEEM experiments, the mean field approach used in homogeneous simulations [4] and the cell size proposed in spatially extended simulations [6,5] were found to be adequate.

From time series behavior, classification of grains of the surface into active and non-active areas naturally emerged. A further classification within the oscillating type I areas was made; i.e., areas displaying homogeneous intensity changes, and areas featuring clustering. The globally multi-peaked reaction rate observed was proven to result from a simple superposition of two types of oscillating grains, rather than from complex feedback coupling of different areas in the polycrystal. We speculate on the existence of these two well-characterized distinct classes to be caused by an uneven distribution of surface defect sites. This assumption is supported by the difference in catalytic activity among the subgroups.

The non-linear nature of time evolution was quantitatively established for this system for the first time to our best knowledge via surrogate data analysis; while correlation dimension calculations carried using GP algorithm allowed to confirm previous results regarding the existence of a subset of 3 *fundamental* variables necessary to describe dynamics, and to speculate on a chaotic underlaying process.

Acknowledgments

Authors gratefully acknowledge J. Lauterbach, and D. Bilbao for providing with detailed PEEM and QMS experimental information used in the present analysis. This work was partially carried while one of the authors (M.R.) was visiting Prof. Imbihl group at Leibniz University of Hannover; the kind hospitality and stimulating discussions are most appreciated. Financial support provided by UNLP (Universidad Nacional de La Plata), CICPBA (Comisión de Investigaciones Científicas de la Prov. de Buenos Aires – Argentina) and CONICET (Consejo de Investigaciones Científicas y Tecnológicas – Argentina) is acknowledged.

References

[1] G. Veser, F. Esch, R. Imbihl, Cat. Lett. 13 (1992) 371.
[2] S.J. Lombardo, T. Fink, R. Imbihl, J. Chem. Phys. 9 (8) (1993) 5526.
[3] M.F.H. van Tol, J. Siera, P. Cobden, B.E. Nieuwenhuys, Surf. Sci. 274 (1992) 63.
[4] H. Uecker, R. Imbihl, M. Rafti, I.M. Irurzun, J.L. Vicente, E.E. Mola, Chem. Phys. Lett. 382 (2003) 232.
[5] M. Rafti, J.L. Vicente, H. Uecker, R. Imbihl, Chem. Phys. Lett. 421 (2006) 577.
[6] H. Uecker, Phys. D 190 (2004) 249.
[7] H. Uecker, Phys. Rev. E 71 (2005) 016207.
[8] H. Haken, Naturwissenschaften 67 (1980) 121.
[9] R. Imbihl, G. Ertl, Chem. Rev. 95 (1995) 697.
[10] R. Imbihl, Surf. Sci. 603 (2009) 1671.
[11] P. Grassberger, I. Procaccia, Phys. Rev. Lett. 50 (1983) 346.
[12] T. Schreiber, Phys. Rep. 308 (1999) 1.
[13] C.G. Takoudis, L.D. Schmidt, J. Chem. Phys. 87 (1983) 958.
[14] C.G. Takoudis, L.D. Schmidt, J. Chem. Phys 87 (1983) 964.
[15] T. Katona, G.A. Somorjai, J. Chem. Phys 96 (1992) 5465.
[16] N. McMillan, C. Snively, J. Lauterbach, Surf. Sci. 601 (2007) 772.
[17] J.M. Bradley, A. Hopkinson, D.A. King, Surf. Sci. 371 (1997) 255.
[18] M. Rafti, F. Lovis, Y.F. Zeng, R. Imbihl, Chem. Phys. Lett. 446 (2007) 323.
[19] M. Gruyters, D.A. King, J. Chem. Soc. Faraday Trans. 93 (1997) 2947.
[20] G. Ertl, Science 254 (1991) 1750.
[21] J.V. Barth, Surf. Sci. Rep. 40 (2000) 75.
[22] A. Makeev, R. Imbihl, J. Chem. Phys. 113 (2000) 3854.
[23] A. Makeev, M. Himz, R. Imbihl, J. Chem. Phys. 114 (2001) 9083.
[24] M. Ding, C. Grebogi, E. Ott, T. Sauer, J.A. Yorke, Phys. Rev. Lett. 70 (1993) 3872.
[25] M. Rafti, J.L. Vicente, Información Tecnológica 21 (2010) 11.
[26] A.R. Osborne, A. Provenzale, Phys. D 35 (1989) 357.
[27] P.E. Rapp, A.M. Albano, T.I. Schmah, L.A. Farwell, Phys. Rev. E 47 (1993) 2289.
[28] J. Theiler, S. Eubank, A. Longtin, B. Galdrikian, J.D. Farmer, Phys. D 5 (8) (1992) 77.
[29] C. Diks, J.C. van Houwelingen, F. Takens, J. DeGoede, Phys. Lett. A 20 (1) (1995) 221.